energies

MDPI

Article

Tracking Control of Modular Multilevel Converter Based on Linear Matrix Inequality without Coordinate Transformation

Ming Liu [1,2], Zetao Li [1,*] and Xiaoliu Yang [1]

[1] College of Electrical Engineering, Guizhou University, Guiyang 550025, China; weiminxiaohai@163.com (M.L.); xlyang1@gzu.edu.cn (X.Y.)

[2] Department of Mechanical Engineering, Guizhou College of Electronic Science and Technology, Guian 550003, China

* Correspondence: ztli@gzu.edu.cn

Received: 25 February 2020; Accepted: 13 April 2020; Published: 16 April 2020



Abstract: Modular multilevel converters (MMCs) play an important role in the power electronics industry due to their many advantages such as modularity and reliability. However, one of the challenges is to suppress fluctuations of circulating current and capacitor voltage and to ensure the quality of the output current. In this paper, the upper and lower arm voltages are employed as control inputs to control the output current and circulating current which are fed back to track the desired value. Based on linear matrix inequality (LMI), the control law of the MMC with multi-input system is designed to optimize the control value. The optimum arm voltage is divided by the SM nominal capacitor voltage to determine the number of SMs inserted into the upper/lower arm. The Voltage Sorting Algorithm (VSA) is then used to suppress the capacitor voltage fluctuation. The proposed tracking control strategy is implemented in MATLAB/Simulink. The results show that even under a small number of SMs (4 per arm), the output current can track the desired values and have better harmonic performance (current THD: 5.42%,voltage THD: 5.67%), and the fluctuations of the circulating current can be suppressed. Furthermore, it has better robustness and three-phase variable load fault tolerance.

Keywords: modular multilevel converter (MMC); tracking control; linear matrix inequality (LMI); circulating current; multi-input system

1. Introduction

With the development of power electronics technology, the modular multilevel converter (MMC) has received extensive attention [1–3]. In recent years, due to its modularity, scalability, high efficiency, good harmonic performance, fault blocking capability, etc., it has been used more and more in the industry [4–8], such as energy storage system, medium voltage and high power motor drive system, power distribution system, high voltage direct current transmission, and so on.

However, it is more challenging than other multilevel converters in the control of an MMC to guarantee the quality of the output current and voltage, at the same time, to minimize/eliminate circulating current while the capacitor voltages were maintained balanced [9]. In other words, when the MMC operates as an inverter, three control objectives need to be met to ensure normal operation. First, the output current or voltage must be controlled at the appropriate amplitude, frequency, and phase. Second, the circulating current flowing through each phase of the MMC must be controlled to a certain value. Third, the capacitor voltage of each SM must maintain its reference voltage [1,6,10].

In the past few years, a variety of control strategies have been proposed/studied. Among them, model predictive control (MPC) has developed rapidly because of its simple implementation, the ability

to control multiple objectives in a cost function and excellent dynamic response [9,10]. However, as the number of SMs rises, its computational complexity is raised exponentially. Fortunately, some scholars have been trying to find ways to reduce the computational load [11–13]. In [14], on the premise that SM capacitor voltage is completely equal, simple linear controllers are employed to regulate the output and inner differential currents of the MMC by feedback linearization-based current control strategy. Proportional integral (PI) and phase shift resonant controller (PR) are based on linear system theory and need to transform abc/dqo and dqo/abc coordinate systems, and need to adjust multiple parameters [1]. Phase Shift Pulse Width Modulation (PS-PWM) [15,16] is suitable for a small number of SM. It has good output voltage and current quality, but the switching frequency is high, which takes up a lot of hardware resources and consumes a lot of energy. Compared with PS-PWM, nearest level control (NLC) [17] is simpler, with lower switching frequency and less loss. When the number of SM is relatively small, the quality of its output voltage and current is poor and the voltage fluctuation of SM capacitors is large. However, as the number of SMs increases, the output quality of the NLC is sufficient. In [18], by adding a small offset that alternates with a double fundamental frequency to the reference signal, the step change moment between the upper and lower arm voltages shows a small phase shift. References [19–22] improved the shortcomings of NLC at low level and achieved some results. In reference [23], a general analysis model and an improved arm control for the modular multilevel converter under asymmetrical operation conditions are proposed.

In view of the shortcomings of the above control methods, this paper proposes a controller that can optimize multi-target control and achieve dynamic tracking. In addition, the complexity of the control system, dynamic response, output current quality and commutation suppression are not affected by the number of SMs.

The structure of this paper is as follows. Section 2 introduces the topology, working principle and mathematical model of MMC. Controller design based on linear matrix inequality are explained in Section 3. The simulation and verification results are shown in Section 4. The conclusions of the study are presented in Section 5.

2. Topology and Mathematical Model of the MMC

2.1. Topology and Principles of Operation

The circuit structure of three-phase MMC is shown in Figure 1, and its single-phase consists of an upper and a lower arm. Each arm is composed of N sub-modules (SM), an inductor and equivalent resistance in series. Individual SM consists of a capacitor C and two complementary IGBT modules (i.e., $T_{jm,n}= \{0,1\}$ and $T'_{jm,n}= \{1,0\}$). In this paper, the subscripts: $j = a, b, c$ means three-phase, $m = u, l$, (u as upper arm, and l as lower arm), n = 1, 2, 3, …, N, which represents the number of sub-modules. The L_j is the arm inductance, and the R_j is the arm equivalent resistance. The u_{jm} and i_{jm} represent the voltage and current of the upper arm or lower arm of phase-j, respectively. The u_{oj} and i_{oj} denote the output voltage and current of phase-j, respectively. The i_{cj} is the circulating current of phase-j. The L_{oj} and Z_j are the inductance and load of phase-j, respectively. The U_{dc} is the DC source voltage. The $u_{SM,jm,n}$ is the nth capacitor voltage of the upper or lower arms of phase-j.

2.2. Mathematical Model of the MMC

According to the structure principle of MMC mentioned above, the relationship between the capacitance voltage and the arm current in phase-j and switching function($T_{jm,n}$) is as follows:

$$\frac{du_{SM,jm,n}}{dt} = T_{jm,n} i_{jm} \tag{1}$$

The relationship between the arm voltage and the capacitor voltage in phase-j and switching function is as follows:

$$u_{jm} = \sum_{n=1}^{N} T_{jm,n} u_{SM,jm,n} \tag{2}$$

Considering the assumed DC-side midpoint in Figure 1, and using the Kirchhoff's circuit law, the following mathematical equations controlling the dynamic characteristics of MMC in phase-j can be obtained:

$$u_{ju} + R_j i_{ju} + L_j \frac{di_{ju}}{dt} + u_{oj} + L_{oj} \frac{di_{oj}}{dt} - \frac{U_{dc}}{2} = 0 \tag{3}$$

$$u_{jl} + R_j i_{jl} + L_j \frac{di_{jl}}{dt} - u_{oj} - L_{oj} \frac{di_{oj}}{dt} - \frac{U_{dc}}{2} = 0 \tag{4}$$

$$i_{oj} = i_{ju} - i_{jl} \tag{5}$$

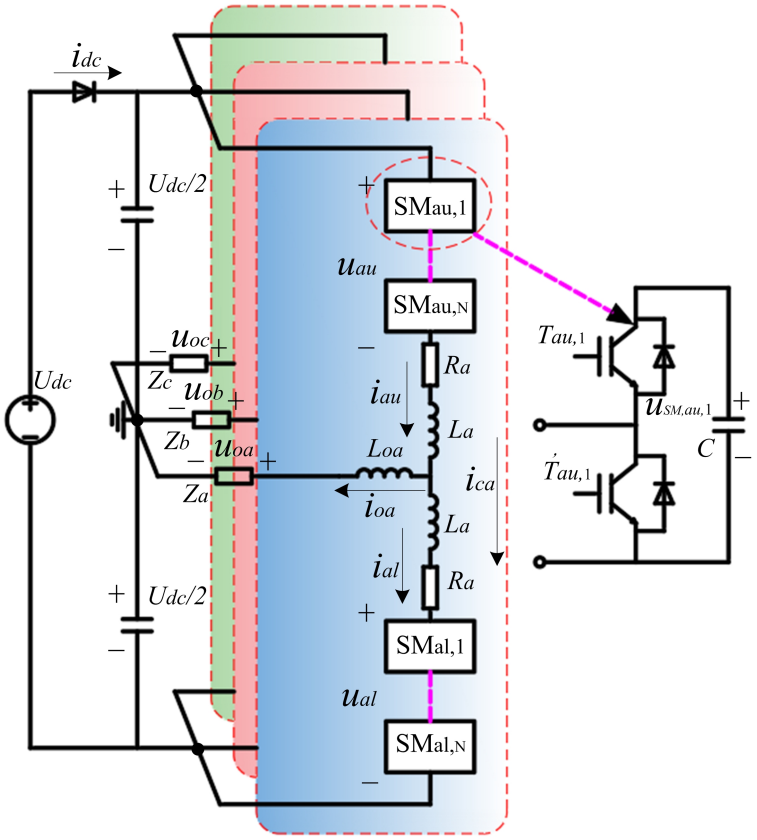


Figure 1. Structure of a three-phase MMC-based inverter and its SM.

Based on Figure 1, the arm currents can be expressed as follows [24]:

$$i_{ju} = \frac{i_{oj}}{2} + i_{cj},\ i_{jl} = \frac{-i_{oj}}{2} + i_{cj} \tag{6}$$

where i_{cj} is the circulating currents flowing through the MMC phase-j, which can be obtained by the following formula.

$$i_{cj} = \frac{i_{ju} + i_{jl}}{2} \tag{7}$$

By the difference between Equations (3) and (4) and substituting for $i_{ju} - i_{jl}$ from Equation (5), the dynamics of phase-j AC-side currents is obtained as follow:

$$\frac{di_{oj}}{dt} = -\frac{R_j}{L_j + 2L_{oj}} i_{oj} - \frac{1}{L_j + 2L_{oj}} u_{ju} + \frac{1}{L_j + 2L_{oj}} u_{jl} - \frac{2}{L_j + 2L_{oj}} u_{oj} \tag{8}$$

Similarly, the dynamic behavior of the circulating current in phase-j is obtained by adding Equations (3) and (4) and substituting for $i_{ju} + i_{jl}$ from Equation (7), and it is expressed as follow:

$$\frac{di_{cj}}{dt} = -\frac{R_j}{L_j} i_{cj} - \frac{1}{2L_j} u_{ju} - \frac{1}{2L_j} u_{jl} + \frac{1}{2L_j} U_{dc} \tag{9}$$

Let $x_1 = i_{oj}, x_2 = i_{cj}, u_1 = u_{ju}, u_2 = u_{jl}$, then, the state equations of MMCs in phase-j can be described as follow:

$$\begin{bmatrix} \dot{x}_1 \\ \dot{x}_2 \end{bmatrix} = \begin{bmatrix} -\frac{R_j}{L_j+2L_{oj}} & 0 \\ 0 & -\frac{R_j}{L_j} \end{bmatrix} \begin{bmatrix} x_1 \\ x_2 \end{bmatrix} + \begin{bmatrix} -\frac{1}{L_j+2L_{oj}} & \frac{1}{L_j+2L_{oj}} \\ -\frac{1}{2L_j} & -\frac{1}{2L_j} \end{bmatrix} \begin{bmatrix} u_1 \\ u_2 \end{bmatrix} + \begin{bmatrix} -\frac{2}{L_j+2L_{oj}} & 0 \\ 0 & \frac{1}{2L_j} \end{bmatrix} \begin{bmatrix} u_{oj} \\ U_{dc} \end{bmatrix} \tag{10}$$

Obviously, Equation (10) is a coupled state equation with multiple control inputs and disturbances. Especially important, the state variables are sinusoidal or cosine functions of periodic fluctuations, which makes the control more difficult. Because there is switching function and strong nonlinearity in SM, MMC model is established by using MATLAB/SIMULINK to solve the capacitor voltage value for replacing Equation (1).

3. Controller Design Based on Linear Matrix Inequality

In the previous section, we have obtained the state equation of MMC, see Equation (10). Then the next task is how to design the control variables u_1 and u_2 so that the desired value of x_1 is sinusoidal and the desired value of x_2 is constant. The ultimate goal of the control is that the output voltage can track the desired value. Since there is no coordinate transformation, the desired value of tracking is a nonlinear function, the LMI is employed for controller design.

3.1. Tracking Controller Design

In this section, based on the developed state model, a systematic controller design methodology is proposed, which is used to control the state variables to follow the desired values. Rewrite Equation (10) as follows:

$$\dot{x} = Ax + Bu + Ey \tag{11}$$

where $x = [x_1, x_2]^T$ is the state vector, $\dot{x} = [\dot{x}_1, \dot{x}_2]^T$ is the time derivative of the state vector, $u = [u_1, u_2]^T$ is the control input vector, $y = [y_1, y_2]^T$ is the disturbance vector. In addition, the state matrix A, the control matrix B, the coefficient matrix E are as follows:

$$A = \begin{bmatrix} a_{11} & 0 \\ 0 & a_{22} \end{bmatrix}, B = \begin{bmatrix} b_{11} & -b_{11} \\ b_{22} & b_{22} \end{bmatrix}, E = \begin{bmatrix} 2b_{11} & 0 \\ 0 & -b_{22} \end{bmatrix} \tag{12}$$

where

$$a_{11} = -\frac{R_j}{L_j + 2L_{oj}}, a_{22} = -\frac{R_j}{L_j}, b_{11} = -\frac{1}{L_j + 2L_{oj}}, b_{22} = -\frac{1}{2L_j}. \tag{13}$$

Assuming that the desired value of x is $x_d = [x_{1d}, x_{2d})]^T$, the error between x and x_d is e, and that the desired value of y is $y_d = [y_{1d}, y_{2d}]^T$, the error between y and y_d is $e_y = [e_{1y}, e_{2y}]^T$, then

$$e = x_d - x \tag{14}$$

$$e_y = y_d - y \tag{15}$$

Deriving time from both sides of Equation (14)

$$\dot{e} = \dot{x_d} - \dot{x} \tag{16}$$

Deriving time from both sides of Equation (15)

$$\dot{e_y} = \dot{y_d} - \dot{y} \tag{17}$$

The goal is to converge the error to zero, i.e., $e, e_y \to 0$ as $t \to \infty$. Assume the control law is as follows:

$$u = Fx - Fx_d - B^{-1}Ax_d - B^{-1}Ey_d + B^{-1}\dot{x}_d \tag{18}$$

where F is feedback gain, which can be obtained by designing LMI. B^{-1} is the inverse of B (invertible).

Take Equation (18) to into Equation (11) get the following equation:

$$dotx_d - \dot{x} = (A + BF)(x_d - x) + E(y_d - y) \tag{19}$$

take Equations (14), and (15) into Equation (19) to get the following equation:

$$\dot{e} = (A + BF)e + Ee_y \tag{20}$$

let Equation (17) equal to:

$$\dot{e_y} = Ne_y \tag{21}$$

where $N = diag(N_1.N_2)$ is feedback gain, which can be obtained by designing LMI.

Theorem 1. *If the following LMIs are satisfied,*

$$\begin{bmatrix} A^TP + M^T + PA + M & PE \\ E^TP & N^T + N \end{bmatrix} < 0,\ P = P^T > 0,\ N^T + N < 0 \tag{22}$$

where $F = (PB)^{-1}M$, then the closed-loop system composed of the system in Equation (11) and the control law in Equation (18) is asymptotically stable.

Proof. Consider the following Lyapunov function candidate.

$$V(e, e_y) = e^TPe + e_y^Te_y \tag{23}$$

where P is a positive definite matrix. The derivative of Equation (23) along Equations (20) and (21) is given by

$$\dot{V} = e^T(A^T + F^TB^T)Pe + e_y^TE^TPe + e^TP(A + BF)e + e^TPEe_y + e_y^T(N^T + N)e_y = Y^T\Omega Y \tag{24}$$

where $Y = [e^T, e_y^T]^T$, and $\Omega = \begin{bmatrix} A^TP + M^T + PA + M & PE \\ E^TP & N^T + N \end{bmatrix}$. To ensure $\dot{V} < 0$, only $Y^T\Omega Y < 0$, i.e., $\Omega < 0$, i.e.,

$$\Omega = \begin{bmatrix} A^TP + M^T + PA + M & PE \\ E^TP & N^T + N \end{bmatrix} < 0 \tag{25}$$

In LMI Equation (25), since both F and P are unknown, in order to solve the LMI, it is necessary to linearize the formula and let $M = PBF$. In addition, the convergence of e_y should be guaranteed, then $N^T + N < 0$. At this time, LMIs were expressed as

$$\begin{gathered} \begin{bmatrix} A^TP + M^T + PA + M & PE \\ E^TP & N^T + N \end{bmatrix} < 0, \\ P > 0,\ N^T + N < 0 \end{gathered} \tag{26}$$

P, M, N can be obtained from Equation (26), thus F can be obtained. Therefore, under the control law in Equation (18), the optimal control can be obtained by LMI if the system is controllable in Equation (11). □

3.2. Relevant Parameters of the Control System

To appraise the performance for the control method, a detailed switch model for three-phase MMC with 8 SM (9 level) in each arm was simulated. The control block diagram of the MMC is shown in Figure 2, and the parameters of the MMC are listed in Table 1.

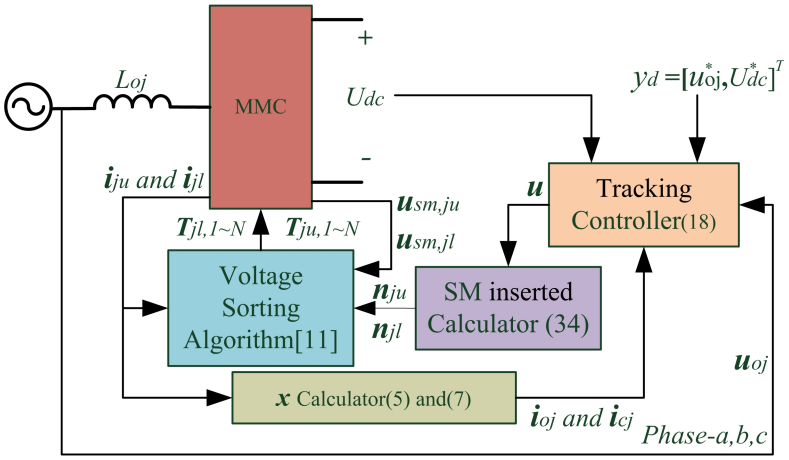


Figure 2. Tracking control block diagram of the study system.

Table 1. Parameters of the study system.(note:* represents desired value).

Name	Parameter (Units)	Value
AC system frequency	f (Hz)	50
AC voltage RMS	U_m^* (V)	1768
AC output voltage of phase-a	u_{oa}^* (V)	$\sqrt{2}U_m^* \cos(2f\pi t)$
DC voltage	U_{dc}^* (V)	6000
nominal capacitor voltage	u_C (V)	750
SM number in each arm	N	8
SM capacitance	C (F)	0.004
Arm inductance	L_j (H)	0.003
Arm equivalent resistance	$R_j(\Omega)$	0.4
equivalent inductance	L_{oj} (H)	0.004

In Figure 2, the desired value is $y_d = [u_{oj}^*, U_{dc}^*]^T$. When the AC side is a passive network, the DC voltage U_{dc} is constant, $U_{dc} = U_{dc}^*$, when the active network, the AC voltage u_{oj} equals u_{oj}^*. F and N is calculated by LMI matrix Equation (22) as follows:

$$\boldsymbol{F} = \begin{bmatrix} 2.8318 & 1.2994 \\ -2.1718 & 0.9966 \end{bmatrix}, \boldsymbol{N} = \begin{bmatrix} -0.4772 & 0 \\ 0 & -0.4781 \end{bmatrix} \tag{27}$$

Therefore, $N_1 = -0.4772$, $N_2 = -0.4781$. In the control system Equation (18), $x_{2d} = 0$ and $\dot{x}_{2d} = 0$, but x_{1d} and $\dot{x}_{1d}$ are unknown. In the following Equations (28)–(33), the k_1, k_2 are real parameters, which are unknown and can be stabilized by adjusting parameters. When the AC side is a passive network, let

$$x_{1d} = k_1 e_{1y} + k_2 \int e_{1y} dt \tag{28}$$

then,

$$\dot{x}_{1d} = k_1 \dot{e}_{1y} + k_2 e_{1y} \tag{29}$$

take Equation (21) into Equation (29):

$$\dot{x}_{1d} = k_1 N_1 + k_2 e_{1y} \tag{30}$$

When the AC side is an active network, let

$$x_{1d} = k_1 e_{2y} + k_2 \int e_{2y} dt \tag{31}$$

then,

$$\dot{x}_{1d} = k_1 \dot{e}_{2y} + k_2 e_{2y} \tag{32}$$

take Equation (21) into Equation (32)

$$\dot{x}_{1d} = k_1 N_2 + k_2 e_{2y} \tag{33}$$

In Figure 2, the x_d and $\dot{x}_d$ are input to the feedback controller calculated based on Equation (18) to obtain an optimal control u. Then, the inserted SMs number of phase-j upper and lower arms is calculated by Equation (34), n_{ju}, n_{jl}. The switch function is calculated by the Voltage Sorting Algorithm applied in [11] to balance all the capacitor voltages of the MMC $u_{SM,jm,n}$. Due to limited space, it will not be repeated here.

The optimal number of SMs inserted in the MMC is as follows.

$$n_{ju} = \frac{u_1}{u_C}; \; n_{jl} = \frac{u_2}{u_C}; \tag{34}$$

where n_{ju} and n_{jl} the number of SMs inserted in the upper and lower arms of the MMC, respectively and u_C is the nominal capacitor voltage of the SM, as follows.

$$u_C = \frac{U_{dc}}{N} \tag{35}$$

The u obtained in Equation (18) is a continuous function, and after Equation (34), it is discretized by the SM structure of the MMC. This is the characteristic of power electronic circuits, a continuous and discrete hybrid system.

Due to the limited space, the dynamic performance of the system was only studied when the AC side is passive in this paper. However, this control method can be applied to other modes of MMC.

4. Simulation Results and Discussion

The simulation model is built in MATLAB/Simulink according to the block diagram as shown in Figure 2. The simulation parameters are listed in Table 1, and initial value $x(0) = 0$. The control target is that the output voltage is not interfered by the load, the converter is suppressed, and the SMs capacitance voltages are stable. Unless otherwise specified in the subsequent simulation, single-phase parameters refer to phase-a. It is assumed that the DC side is a constant voltage source without fluctuation.

4.1. Tracking Performance Under Desired Value Change

It is assumed that during 0.06–0.14 s, the amplitude value of the desired u_{oj}^* changes to 0.6 times. The simulation results are shown in Figures 3–5.

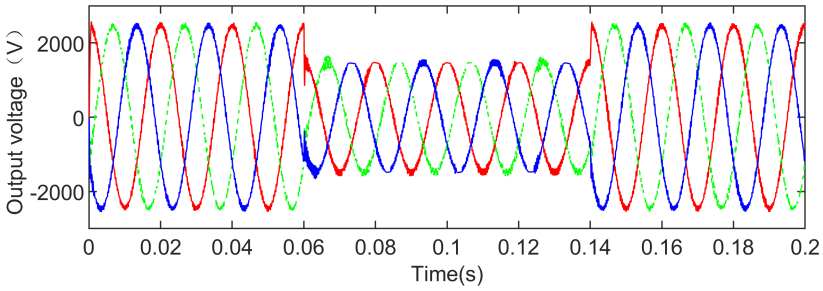


Figure 3. Output voltage (u_{oa}, u_{ob}, u_{oc}) waveforms under desired value change.

In Figure 3, it has been shown that the three-phase voltage with the desired voltage change. The amplitude of the three-phase voltage also change with the desired value, and the change amplitude is also 0.6 times of the original value.

The output voltage of phase-a tracking the desired value is shown in Figure 4. It is obvious that u_{oa} can track u_{oa}^* well and respond quickly even when the desired value u_{oa}^* changes suddenly. And the tracking error (mean value: 11.1347 V, root mean square value: 191.8994 V) has been shown in Figure 5.

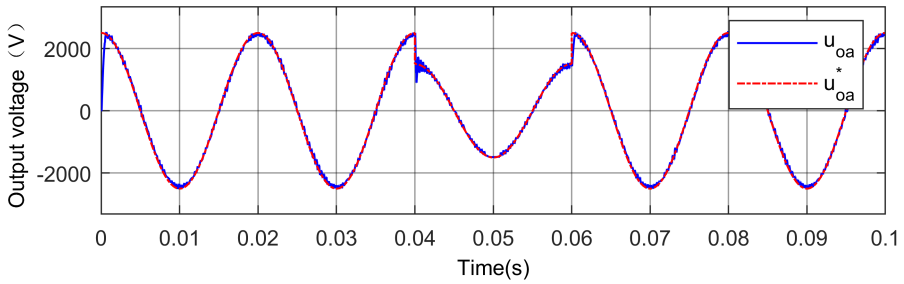


Figure 4. Dynamic performance of output voltage (u_{oa}) tracking its desired value (u_{oa}^*).

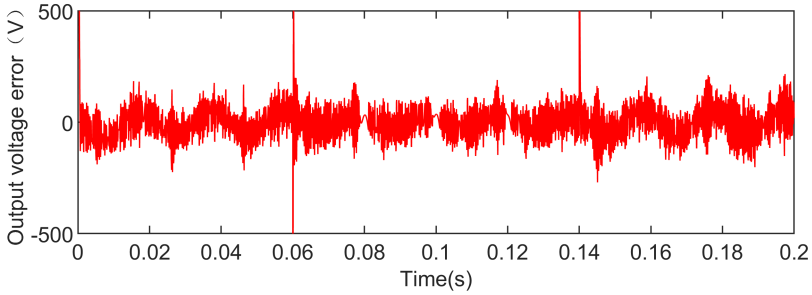


Figure 5. Error of output voltage (u_{oa}) tracking its desired value (u_{oa}^*).

In a word, it can be seen from Figures 3–5 that the follow-up performance of the control system is well.

4.2. Dynamic Performance Under Different Loads

In this section, the stability of output voltage under three-phase symmetrical load is studied. It is assumed that load Z consisted of the resistance and inductance, and its value is shown in Table 2. In four cases, the simulation results of phase-a are shown in Figures 6 and 7. However, the load is not limited to those listed in Table 2, it can be any form, whether linear or nonlinear.

Table 2. Load parameters of the MMC.

Load	Resistance (Ω)	Inductance (mH)
Z1	20	0.1
Z2	10	0.1
Z3	20	0.2
Z4	10	0.2

In Figure 6, it is shown that the output voltage has little change under four load conditions, and the voltage RMS error is shown in Figure 7.

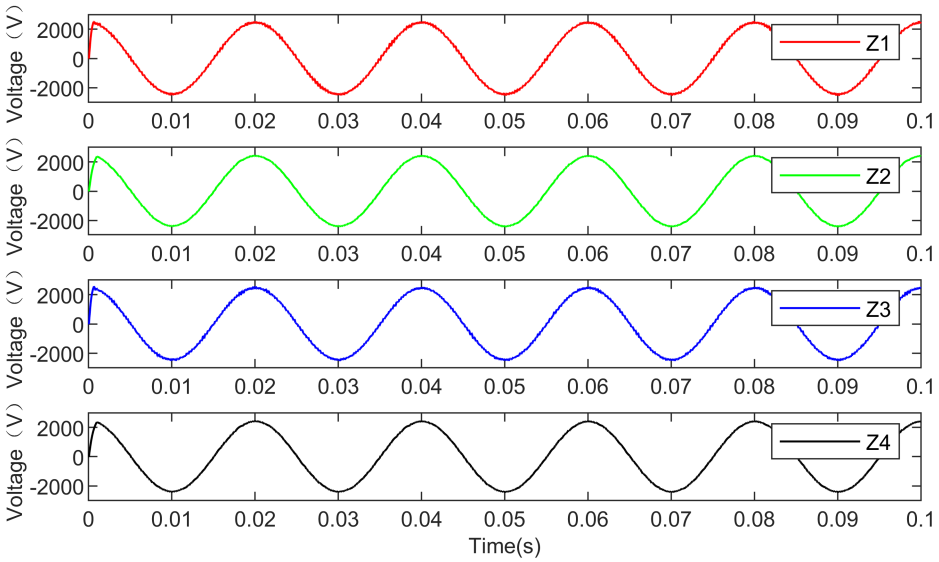


Figure 6. Output voltage waveform under four load conditions.

In Figure 7, Z1 and Z3 fluctuate in a wide range. Z2 and Z4 fluctuate less. It can be seen that the resistance value in the load has a certain influence on the control error, while the inductance value has little influence. If the allowable voltage fluctuation range is assumed to be 10% of the desired value, it is 250 V, with safety margin. Therefore, the proposed control method has been proved to be robust.

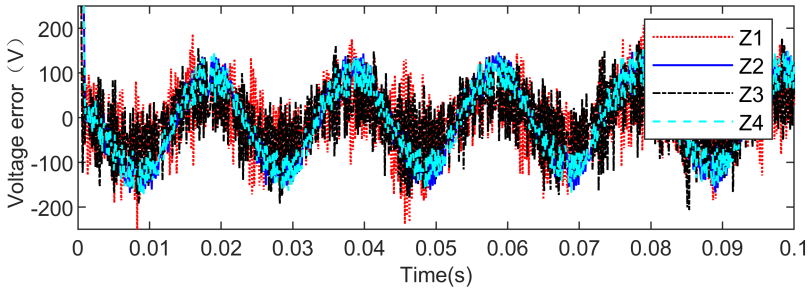


Figure 7. Output voltage RMS error under different loads.

4.3. Fault Tolerance

In the section, the stability of the output voltage has been studied under the condition of three-phase load asymmetry. The simulation parameters are shown in Table 3. There are two cases. In case 1, the load of phase-a is different from phase-b and phase-c. In case 2, the three-phase resistances are different.

Table 3. Load parameters of the MMC.

Case	Phase-j	Resistance (Ω)	Inductance (mH)
case1	a	10	0.1
	b,c	20	0.1
case2	a	20	0.1
	b	15	0.1
	c	10	0.1

The simulation results are shown in Figures 8–11. In Figures 8 and 9, the output current and voltage in case 1 are shown, respectively. Same as this, in Figures 10 and 11, the output current and voltage in case 2 are shown, respectively. From these figures, it can be seen that the output voltage is basically unchanged in either case1or case 2, as shown in Figures 8 and 10. It has been shown that the current decreases as the resistance increases in Figures 9 and 11. This is in accordance with Ohm's law. When the voltage is fixed, the resistance is proportional to the current.

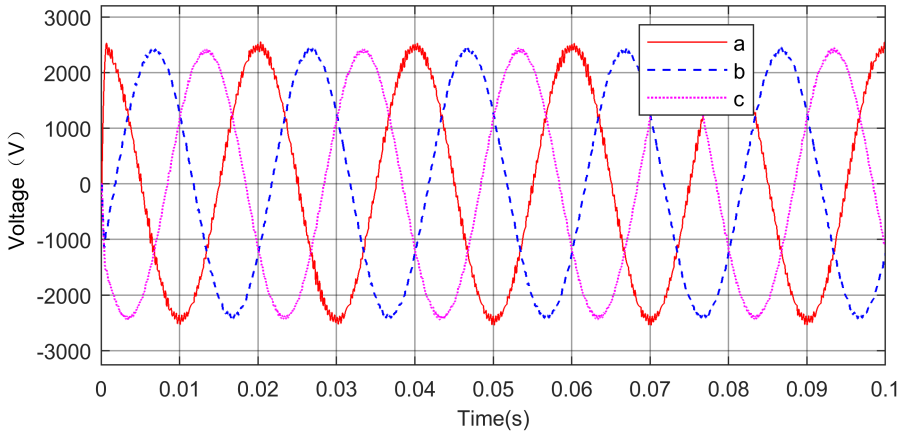


Figure 8. Output three-phase voltage diagram under case 1.

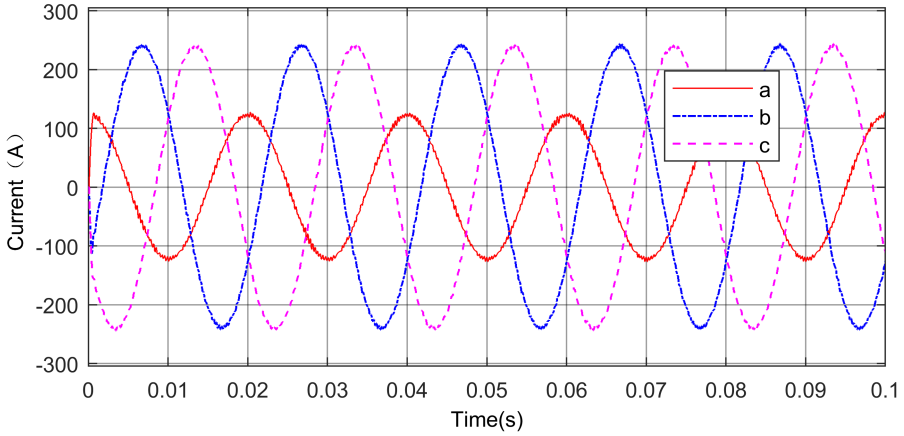


Figure 9. Output three-phase current diagram under case 1.

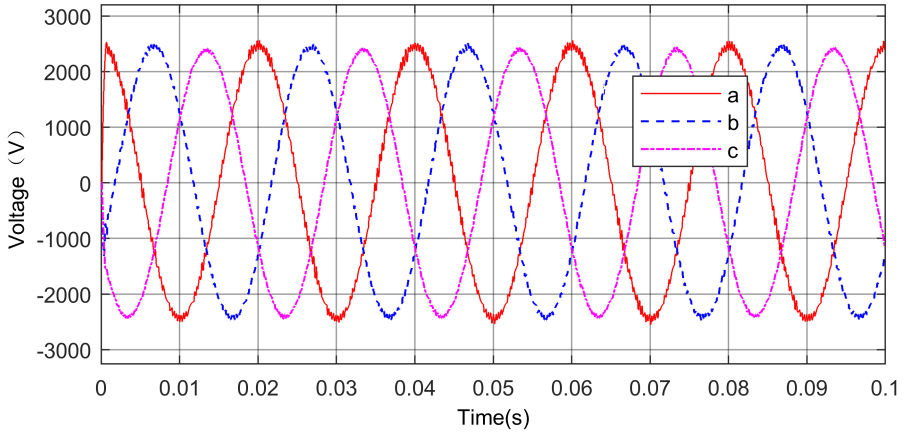


Figure 10. Output three-phase voltage diagram under case 2.

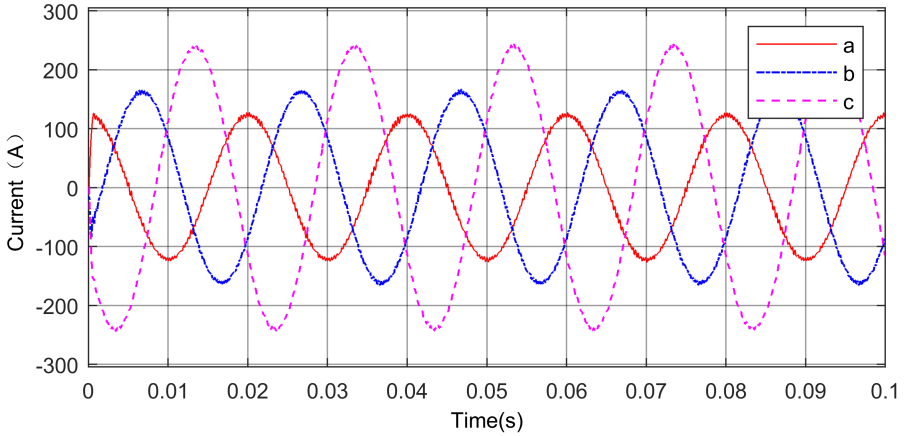


Figure 11. Output three-phase current diagram under case 2.

In short, the proposed control method has no coordinate transformation, so there is no coupling relationship among the three phases, which improves the fault tolerance of the system.

4.4. Dynamic Performance Under Different Number of Sub-Modules

In this section, it has been researched that the application of the proposed control method under different number of SMs. The system parameters are shown in Table 1. To compare the control performance, two cases of 4 SMs (5 level) and 8 SMs (9 level) at each arm are studied. The corresponding capacitance voltage is 1500 V and 750 V, and the other parameters remain unchanged. The simulation results are shown in Figures 12–16.

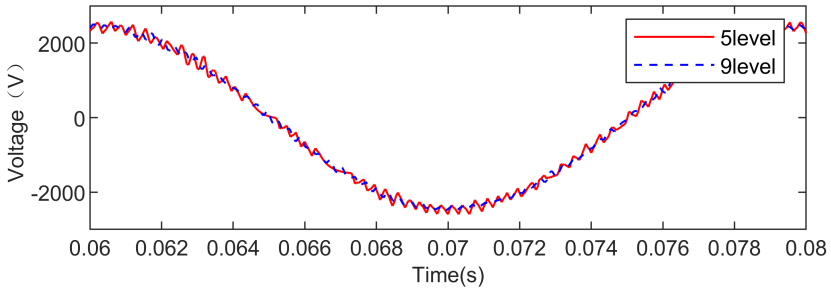


Figure 12. Output voltage (u_{oa}) waveforms.

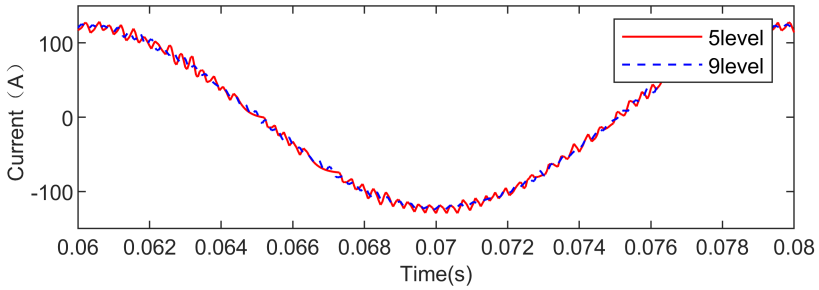


Figure 13. Output current (i_{oa}) waveforms.

The output voltage and current are shown in Figures 12 and 13, respectively. Neither voltage nor current can be completely coincident, and the fluctuation of 5 level is slightly larger.

In Figure 14a,c, the current THD value of 5level is shown 5.42% and the voltage THD value 5.67%, and in Figure 14b,d, the current THD value of 9level is 2.87% and the voltage THD value is 2.99%, respectively. The number of visible levels is doubled, and the THD value is reduced by about half.

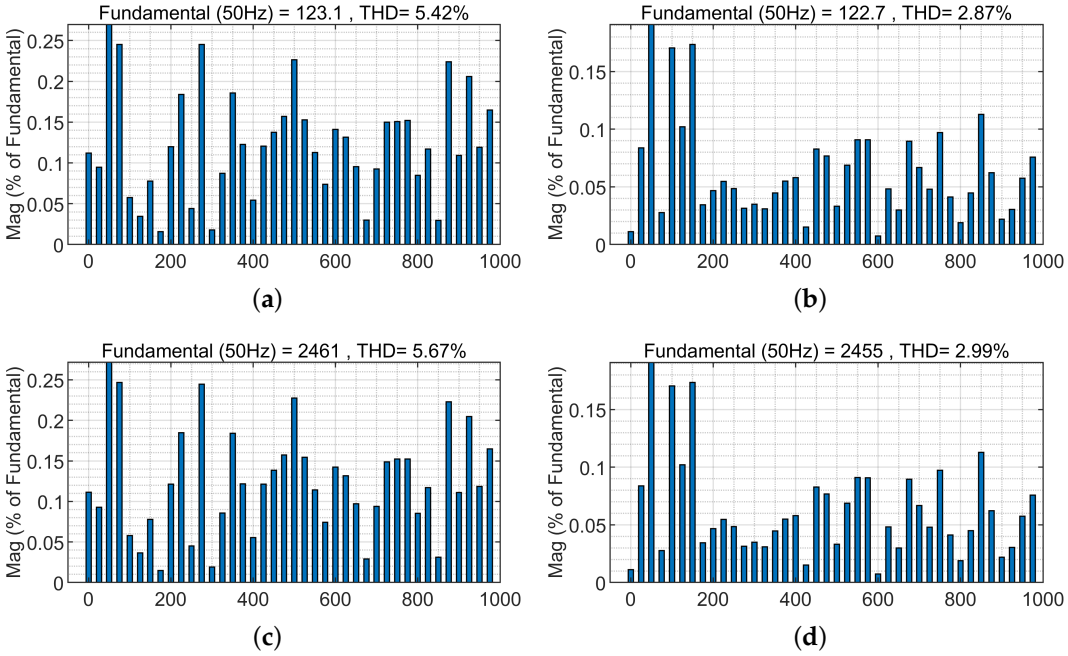


Figure 14. Output current FFT results of two case: (**a**) Output current in 5 level. (**b**) Output current in 9 level. (**c**) Output voltage in 5 level. (**d**) Output voltage in 9 level.

In Figure 15, the circulating current has been suppressed. The mean value of 5 level is 24.6 A, and the standard deviation is 15.5 A. the mean value of 9 level is 25.2 A, and the standard deviation is 25.5 A.

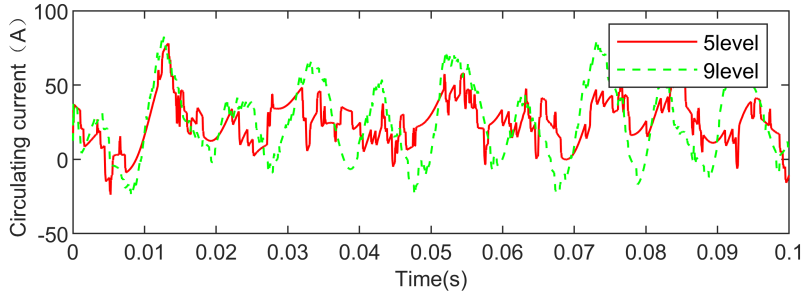


Figure 15. Circulating current (i_{ca}) waveforms of two cases.

In Figure 16a, the SM mean voltage in the upper arm of 5 level is 1490.4 V (lower arm: 1483.3 V), the fluctuation range is −2.66%∼1.21% (lower arm: −2.82%∼0.9%). In Figure 16b, the SM mean voltage in the upper arm of 9 level is 744.0 V (lower arm: 739.6 V), the fluctuation range is −5.51%∼2.63%, (lower arm: −4.43%∼2.63%). Their range is less than 6%. In general, the fluctuation value is considered to be 10∼12% in the design [25].

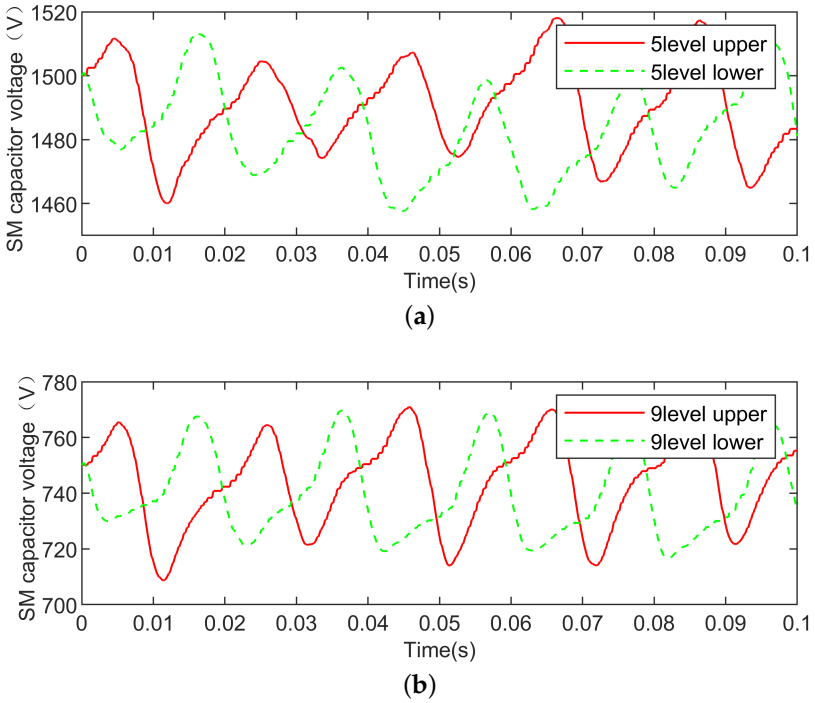


Figure 16. Capacitor voltage $(u_{SM,au,n}, u_{SM,al,n})$ waveforms of two cases: (**a**) one capacitor voltage in upper/lower arm in 5 level. (**b**) one capacitor voltage in upper/lower arm in 9 level.

5. Conclusions

This paper presents a controller design methodology to control the MMC based on LMI method. To describe the dynamic characteristics of AC-side current and circulating current, a multi-input and multi-output mathematical model of the MMC is established. Unlike the traditional control model, the model does not require coordinate transformation. The voltage of the upper(lower) arm is used as a control input to adjust the number of SMs inserted into the upper(lower) arm. Then, according to the output current and the circulating current feedback, the voltage of the upper and lower arms is corrected. Conversely, the voltage of the upper(lower) arm is corrected according to the error between output current and circulating current compared to their respective desired values. However, the desired value of the current is determined by the voltage.

Simulation results are provided to verify the effectiveness of the proposed strategy. It has been proved that the proposed control method has fast response, good robustness, high fault tolerance and can adapt to MMC low-level control by the study of tracking response speed and accuracy, load change, three-phase load asymmetry, different SMs number. More exciting is that the proposed control method only needs to adjust one PI value.

Author Contributions: Conceptualization, M.L. and Z.L.; methodology, M.L.; software, M.L.; validation, M.L.; resources, X.Y.; data curation, X.Y.; writing—original draft preparation, M.L.; writing—review and editing, M.L.; project administration, X.Y.; funding acquisition, Z.L. All authors have read and agreed to the published version of the manuscript.

Funding: This research was funded by the National Natural Science Foundation of China [No. 61963009], and Collaborative Foundation of Guizhou Province [No. 7228(2017)], and Platform Talent Project of Guizhou Province [No. 5788(2017)].

Conflicts of Interest: The authors declare no conflict of interest.

Abbreviations

MMC	modular multilevel converter	LMI	linear matrix inequality
$j = a, b, c$	three-phase	$m = u, l$	u as upper arm, l as lower arm
SM	sub-module	$n = 1, 2, 3 \ldots, N$	N number of SM
$T_{jm,n}(T'_{jm,n})$	switching function	L_j	arm inductance of phase-j
R_j	arm equivalent resistance	u_jm	arm voltage
i_{jm}	arm current	i_{oj}	output current
u_{oj}	output voltage	i_{cj}	circulating current
L_{oj}	equivalent inductance	Z_j	load
U_{dc}	DC source voltage	$u_{SM,jm,n}$	SM capacitor voltage
A	state matrix	B	control matrix
E	coefficient matrix	e, e_y	tracking error
F, N	feedback gain	P	positive definite matrix
k_1, k_2, k_3	real parameters	u_{jm}	inserted SMs' number

References

1. Debnath, S.; Qin, J.; Bahrani, B.; Saeedifard, M.; Barbosa, P. Operation, Control, and Applications of the Modular Multilevel Converter: A Review. *IEEE Trans. Power Electron.* **2018**, *30*, 37–53. [CrossRef]
2. Raju, M.N.; Sreedevi, J.; Mandi, R.P.; Meera, K.S. Modular multilevel converters technology: A comprehensive study on its topologies, modelling, control and applications. *IET Power Electron.* **2019**, *12*, 149–169. [CrossRef]
3. Kouro, S.; Malinowski, M.; Gopakumar, K.; Pou, J.; Franquelo, L.G.; Wu, B.; Rodriguez, J.; Pérez, M.A.; Leon, J.I. Recent advances and industrial applications of multilevel converters. *IEEE Trans. Ind. Electron.* **2010**, *57*, 2553–2580. [CrossRef]
4. Picas, R.; Zaragoza, J.; Pou, J.; Ceballos, S.; Konstantinou, G.; Capella, G.J. Study and comparison of discontinuous modulation for modular multilevel converters in motor drive applications. *IEEE Trans. Ind. Electron.* **2019**, *66*, 2376–2386. [CrossRef]
5. Li, B.; Zhou, S.; Xu, D.; Yang, R.; Xu, D.; Buccella, C.; Cecati, C. An Improved Circulating Current Injection Method for Modular Multilevel Converters in Variable-Speed Drives. *IEEE Trans. Ind. Electron.* **2016**, *63*, 7215–7225. [CrossRef]
6. Perez, M.A.; Bernet, S.; Rodriguez, J.; Kouro, S.; Lizana, R. Circuit Topologies, Modeling, Control Schemes, and Applications of Modular Multilevel Converters. *IEEE Trans. Power Electron.* **2015**, *30*, 4–17. [CrossRef]
7. Li, J.; Konstantinou, G.; Wickramasinghe, H.R.; Pou, J. Operation and Control Methods of Modular Multilevel Converters in Unbalanced AC Grids: A Review. *IEEE J. Emerg. Sel. Topics Power Electron.* **2019**, *7*, 1258–1271. [CrossRef]
8. Nguyen, T.H.; Hosani, K.A.; El Moursi, M.S.; Blaabjerg, F. An Overview of Modular Multilevel Converters in HVDC Transmission Systems with STATCOM Operation during Pole-to-Pole DC Short Circuits. *IEEE Trans. Power Electron.* **2019**, *34*, 4137–4160. [CrossRef]
9. Vatani, M.; Bahrani, B.; Saeedifard, M.; Hovd, M. Indirect Finite Control Set Model Predictive Control of Modular Multilevel Converters. *IEEE Trans. Smart Grid* **2015**, *6*, 1520–1529. [CrossRef]
10. Riar, B.S.; Geyer, T.; Madawala, U.K. Model predictive direct current control of modular multilevel converters: Modelling, analysis, and experimental evaluation. *IEEE Trans. Power Electron.* **2015**, *30*, 431–439. [CrossRef]
11. Gutierrez, B. Modular Multilevel Converters (MMCs) Controlled by Model Predictive Control with Reduced Calculation Burden. *IEEE Trans. Power Electron.* **2018**, *33*, 9176–9187. [CrossRef]
12. Zhou, D.; Yang, S.; Yi, T. Model-Predictive Current Control of Modular Multilevel Converters with Phase-Shifted Pulse width Modulation. *IEEE Trans. Ind. Electron.* **2019**, *66*, 4368–4378. [CrossRef]
13. Liu, P.; Wang, Y.; Cong, W.; Lei, W. Grouping-Sorting-Optimized Model Predictive Control for Modular Multilevel Converter with Reduced Computational Load. *IEEE Trans. Power Electron.* **2016**, *31*, 1896–1907. [CrossRef]

14. Yang, S.; Wang, P.; Tang, Y. Feedback linearization-based current control strategy for modular multilevel converters. *IEEE Trans. Power Electron.* **2018**, *33*, 161–174. [CrossRef]
15. Deng, F.; Chen, Z. Voltage-balancing method for modular multilevel converters under phase-shifted carrier-based pulse width modulation. *IEEE Trans. Ind. Electron.* **2015**, *62*, 4158–4169. [CrossRef]
16. Hagiwara, M.; Akagi, H. Control and experiment of pulse width modulated modular multilevel converters. *IEEE Trans. Power Electron.* **2009**, *24*, 1737–1746. [CrossRef]
17. Meshram, P.M.; Borghate, V.B. A simplified nearest level control (NLC) voltage balancing method for modular multilevel converter (MMC). *IEEE Trans. Power Electron.* **2015**, *30*, 450–462. [CrossRef]
18. Lin, L.; Lin, Y.; He, Z.; Chen, Y.; Hu, J.; Li, W. Improved Nearest-Level Modulation for a Modular Multilevel Converter with a Lower Submodule Number. *IEEE Trans. Power Electron.* **2016**, *31*, 5369–5377. [CrossRef]
19. Wang, Y.; Hu, C.; Ding, R.; Xu, L.; Fu, C.; Yang, E. A Nearest Level PWM Method for the MMC in DC Distribution Grids. *IEEE Trans. Power Electron.* **2018**, *33*, 9209–9218. [CrossRef]
20. Wu, D.; Peng, L. Characteristics of nearest level modulation method with circulating current control for modular multilevel converter. *IET Power Electron.* **2016**, *9*, 155–164. [CrossRef]
21. Li, W.; Hu, J.; Hu, S.; Yang, H.; Yang, H.; He, X. Capacitor Voltage Balance Control of Five-Level Modular Composited Converter with Hybrid Space Vector Modulation. *IEEE Trans. Power Electron.* **2018**, *33*, 5629–5640. [CrossRef]
22. Shen, K.; Wang, S.; Zhao, D.; Zhao, G.A. Discrete-Time Low-Frequency-Ratio Nearest Level Modulation Strategy for Modular Multilevel Converters with Small Number of Power Modules. *IEEE Access* **2019**, *7*, 25792–25803. [CrossRef]
23. Liu, Z.; Miao, S.; Fan, Z.; Chao, K.; Liu, Y. Electrical Power and Energy Systems Characteristics analysis and improved arm control of modular multilevel converter under asymmetric operation conditions. *Electr. Power Energy Syst.* **2019**, *105*, 272–282. [CrossRef]
24. Vatani, M.; Hovd, M.; Maryam, S. Control of the Modular Multilevel Converter Based on a Discrete-Time Bilinear Model Using the Sum of Squares Decomposition Method. *IEEE Trans. Power Del.* **2015**, *30*, 2179–2188. [CrossRef]
25. Zheng, X.; Chen, H.; Pan, W.; Jing, Z.; Xiao, H.; Qingrui, T.; Guan, M.; Zhang, Z.; Pan, W.; Gaoren, L.; et al. Main circuit parameter selection and loss calculation of MMC basic unit. In *HVDC System*, 2nd ed.; Lv, H., Zhu, L., Eds.; China Machine Press: Beijing, China, 2016; pp. 69–71.



© 2020 by the authors. Licensee MDPI, Basel, Switzerland. This article is an open access article distributed under the terms and conditions of the Creative Commons Attribution (CC BY) license (http://creativecommons.org/licenses/by/4.0/).